



Article

The Dynamics Characteristics of Soil Water Infiltration and Capillary Rise for Saline–Sodic Soil Mixed with Sediment

Chitao Sun ¹, Di Feng ², Chao Yu ¹, Jingsheng Sun ³, Xin Han ⁴, Mingming Zhang ^{1,*} , Peng Zhang ^{1,*},
Huifang Han ¹, Weibing Mao ¹ and Xiaojun Shen ⁴ 

- ¹ College of Water Conservancy and Civil Engineering, Shandong Agricultural University, Tai'an 271018, China; sunchitao@163.com (C.S.); yc961231@163.com (C.Y.); hhf@sdaa.edu.cn (H.H.); maoweibing316@126.com (W.M.)
 - ² School of Agronomy and Environment, Weifang University of Science and Technology, Weifang 262700, China; fengdi2008sunny@163.com
 - ³ Key Laboratory of Crop Water Use and Regulation, Ministry of Agriculture, Farmland Irrigation Research Institute, Chinese Academy of Agricultural Sciences, Xinxiang 453000, China; jshsun623@163.com
 - ⁴ College of Hydraulic Engineering, Tianjin Agricultural University, Tianjin 300384, China; xinhhan@tjau.edu.cn (X.H.); shenxiaojun8003@163.com (X.S.)
- * Correspondence: zhangmingming1990@126.com (M.Z.); tazhangpeng@163.com (P.Z.); Tel.: +86-156-8476-2957 (M.Z.)

Abstract: Yellow River sediment is the potential resource for saline–sodic soil reclamation. Experiments of one-dimensional soil columns were conducted to investigate the upward and downward soil water transportation characteristics for saline–sodic soil mixed with different sediment addition (0, 10, 20 kg/m² in the top 20 cm layer). The saturated hydraulic conductivity, ratio of macroporosity, cumulative capillary adsorption and infiltration rate all increased with the increase in sediment addition. No significant differences were detected for both the initial capillary rise rate and the initial infiltration rate for the upward and downward water transportation treatments, respectively. The average adsorption and infiltration rates showed an increasing trend with the increased sediment addition. The initial and average infiltration rates were higher than the initial capillary rise rate and average adsorption rates. The Philip model seems the optimal choice for the dynamic simulation of both upward and downward soil water transportation. The results may provide useful information for soil salinization amelioration.

Keywords: saline–sodic soil; sediments; water movement; dynamic model



Citation: Sun, C.; Feng, D.; Yu, C.; Sun, J.; Han, X.; Zhang, M.; Zhang, P.; Han, H.; Mao, W.; Shen, X. The Dynamics Characteristics of Soil Water Infiltration and Capillary Rise for Saline–Sodic Soil Mixed with Sediment. *Water* **2022**, *14*, 481. <https://doi.org/10.3390/w14030481>

Academic Editors: Qiang Fu, Yongqiang Cao, Tianxiao Li and Mo Li

Received: 4 January 2022

Accepted: 4 February 2022

Published: 6 February 2022

Publisher's Note: MDPI stays neutral with regard to jurisdictional claims in published maps and institutional affiliations.



Copyright: © 2022 by the authors. Licensee MDPI, Basel, Switzerland. This article is an open access article distributed under the terms and conditions of the Creative Commons Attribution (CC BY) license (<https://creativecommons.org/licenses/by/4.0/>).

1. Introduction

The Yellow River Delta is one of the three major estuary deltas in China, which plays an important role in the ecological environment construction and conservation [1–3]. The saline–sodic land in this region is about 2.36×10^5 hm², which accounts for more than 30% of the total delta region's area [4]. In the delta region, the soils have high salinity (with an electrical conductivity more than 20 dS/m for saturated extract), with an average sodium adsorption ratio (SAR) of more than 30 (mmol/L)^{0.5} and an exchangeable sodium percentage (ESP) of more than 20%; moreover, a low ratio of precipitation (580 mm annual on average) to evaporation (1880 mm annual on average) as well as the shallow groundwater table (0.5–1.5 m deep) exacerbates salinization [5]. Indeed, soil permeability is seriously blocked due to the poor soil particle distribution [6]. It is necessary to take proper measures to improve and reduce the current saline–sodic soil for this region.

In order to prevent salt accumulation and increase desalinization, various materials are used for soil water and salt transportation management in saline–sodic soils [7–9]. Li et al. [10] found that in the semi-arid loess region of Northwest China, the use of a gravel-sand effectively reduced soil evaporation and runoff and highly improved soil

infiltration and temperature. Sun et al. [11] found that the soil salinization slowed down as the capillary rise was cut off after a gravel sand layer was embedded in the soil in North China. In the Huang Huai Hai plain of China, Zhang et al. [12] found that punching sediment could increase the water infiltration rate of the saline–sodic soil. There are about 1.08×10^9 tons of sediments per year transported from the Loess Plateau to the downstream delta by the Yellow River, and only 10–15% of the sediments are transported to the field by irrigation. Most sediments (mainly silt particles) are deposited on both sides of the riverbed, where ecological problems such as soil desertification and sandstorms often occur [13,14]. Because the sand particle content is relatively high and the available water is low for the sediment, how to deal with the accumulated sediments remains a serious problem [15–17]. Previous studies have shown that sediment addition can change both the soil particle composition ratio and soil texture, thus changing the water and salt transport pattern of saline–sodic soil [18,19]. On the other hand, sediment addition can enhance the soil aggregate structure and increase the soil water retention and storage capacity [20,21]. Therefore, sediment addition to the soil can not only increase the infiltration capacity of soil but can also increase the water content of soil below the sediment addition layer, which can effectively inhibit the evaporation of soil water and the accumulation of salt in the surface layer [22]. However, the improvement mechanism of sediment on saline–sodic soil and the dynamic characteristics of soil water and salt movement after sediment addition are not clear.

Modeling is widely accepted for its convenience and labor-saving. The accurate performance of the soil water transportation is of critical importance in hydrological modeling. Numerous water transportation models have been established in the past 100 years, such as the Green–Ampt, Kostiakov, Horton and Philip models [23–27], and they are tested and evaluated under various conditions [26,27]. However, most of the previous studies mainly paid attention to the influence of soil texture, vegetation cover and rainfall intensity and seldom considered the impacts of layered soil which were influenced by human activity or natural disturbance [27–29]. Finding the proper water transportation models for layered soil is critical for soil water management and saline–sodic soil amendment.

We hypothesized that after mixing saline–sodic soil with sediment, the soil pore distribution changes (because there are significant differences in the proportion of soil particles between the two materials) and affects the soil water and salt movement process. Based on the above analysis, the purpose of this study is to evaluate the effects of sediment addition on soil infiltration, the capillary rise process and the soil water and salt transport mechanism of saline–sodic soil. Moreover, the performance of three water transportation models (Kostiakov, Horton and Philip) will be evaluated with the addition of sediment. The results can provide a theoretical basis for the improvement of saline–sodic soil by sediment in the Yellow River Delta.

2. Materials and Methods

2.1. Experimental Design

The experiment was conducted in the Water Conservancy and Civil Engineering Center of Shandong Agricultural University from 2018–12 to 2019–03. The air temperature was 12–18 °C and the relative humidity was 17–50% during the experimental period. The soil samples were taken from Bin-Zhou City, Shandong Province (37°17′–38°03′ N, 117°42′–118°04′ E; 4 m above sea level), and the sediments were taken from the settling basin of Xiao Kai He irrigation district (serves as an ideal site for large-scale application of Yellow River sediment). According to our previous investigation, the saline–sodic soil has high clay content and low sand content with a soil salt content of 4.01 g/kg, and the soil texture is sandy clay, while the Yellow River sediment has low clay content and high sand content, and the soil texture of the sediment is loamy fine sand (Table 1). According to the conclusions of Mao et al. and Wang et al. [18,30], three sediment additions (0 kg/m², 10 kg/m² and 20 kg/m²) were mixed with saline–sodic soil in the upper 0–20 cm layer with

a bulk density of 1.35 g/cm^3 to simulate the capillary water rise (upward) and soil water infiltration (downward) process. The experiment included 6 treatments, and each treatment was repeated 3 times. For the capillary water level rise (upward water) treatments, the sediment additions of 0 kg/m^2 , 10 kg/m^2 and 20 kg/m^2 were named U0, U10 and U20, respectively. Correspondingly, the soil water infiltration (downward water) treatments were D0, D10 and D20, respectively. Therefore, both U10 and D10 and U20 and D20 have the same soil physical properties (Table 1).

Table 1. Soil physical properties for different treatments.

Treatments	Soil Texture	Percentage of Particle Content (%)			pH	ECe (dS/m)	Organic Matter (g/kg)	Total N (g/kg)	ESP (%)
		Clay 0–2 μm	Silt 2–50 μm	Sand 50–2000 μm					
Sediment	Loamy Fine Sand	0.39	22.91	76.69	7.6	1.78	12.42	1.42	28.7
U0/D0	Sandy Clay	35.13	19.25	45.62	8.2	6.52	3.28	0.47	10.2
U10/D10	Sandy Clay	35.49	18.34	46.17	8.2	6.47	3.35	0.51	10.1
U20/D20	Sandy Clay	36.07	16.64	47.29	8.1	6.50	3.61	0.56	9.7

Note: Soil particles were measured with pipette sampling method; ECe is the electrical conductivity for saturate soil; ESP is the exchangeable sodium percentage.

Plexiglass tubes with uniform perforation at the bottom (aperture 1.5 mm) were prepared for the experiment, and the tubes were 14 cm in inner diameter and 60 cm in height with a thickness of 0.5 cm. A gravel-sand (2–3 mm in diameter) layer was placed at the bottom of the column, and filter paper was placed between the saline-sodic soil and the gravel-sand filter layer to prevent mixing. The gravel-sand was cleaned with diluted hydrochloric acid and distilled water before the experiment. The saline-sodic soil was filled in layers (5 cm at a time) to a height of 50 cm, and there was a 5 cm space reserved at the top of the plexiglass column (Figure 1). The soils and sediments were air-dried, crushed and passed through a 2 mm sieve before being statically compacted. The water head height is maintained at 5 cm for one-dimensional ponding infiltration, controlled by Mariotte bottle. The gravel-sand was immersed in the beaker to simulate the capillary rise of groundwater under natural conditions. The outlet of the Mariotte flask was consistent with the gravel-sand surface.

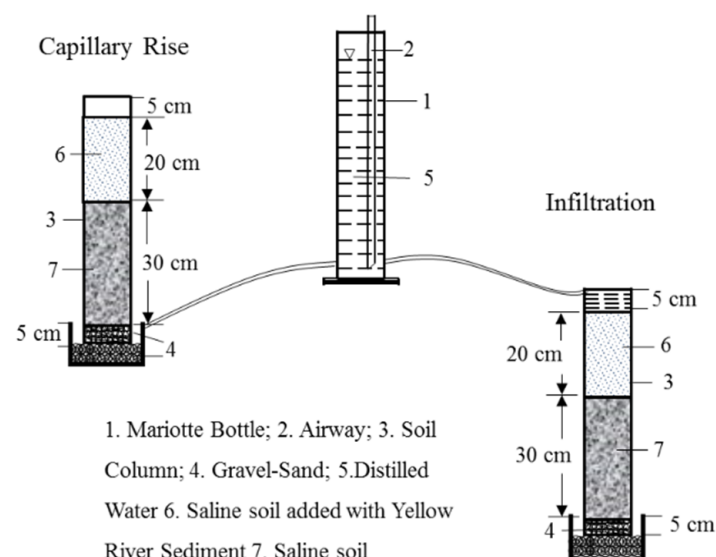


Figure 1. Experimental equipment.

2.2. Simulation Models

The Kostiakov (Equation (1)), Philip (Equation (2)) and Horton (Equation (3)) models corresponding with time were selected to adjust the observed values [23–26]:

$$y = \alpha k x^{\alpha-1} \quad (1)$$

$$y = a + \frac{1}{2} k x^{-0.5} \quad (2)$$

$$y = b + c e^{-\beta x} \quad (3)$$

where y is the infiltration rate (mm/h) and x is the infiltration time (min); α , β , a , b , c and k are statistical parameters of the models and estimated by nonlinear regression using the least squares method.

2.3. Data Collection and Analysis

Saturated hydraulic conductivity for sediment additions of 0, 10 and 20 kg/m² soil samples were measured with Ksat hydraulic conductivity equipment (Germany) based on the falling head method. Soil samples were prepared to the special ring knife (80 mm in inner diameter and 50 mm in height). The samples were saturated with water before measuring, Ksat can be calculated with the Darcy' Law as water passes through the ring knife from the bottom to the top layer at a certain time. Soil porosity is important for water movement, and we regarded pore diameters of 0.2–1 μ m, 1–30 μ m and >30 μ m as microporosity, mesoporosity and macroporosity, respectively, according Nimmo, Rabot et al. [31,32]. Equivalent pore diameter and its porosity ratio calculation can be referred to Equations (4) and (5):

$$d = \frac{4\sigma}{h} \quad (4)$$

$$p = \frac{v_w}{v_s} \times 100\% \quad (5)$$

where d represents diameter of permeable pore, μ m; σ means surface tension of water, 75×10^{-5} N/cm; h means soil water potential, cm; p means soil porosity ratio, %; v_w means soil water volume discharged above the corresponding soil water potential, cm³; v_s means volume of soil sample, cm³.

For pore diameters of 0.2–1 μ m, 1–30 μ m and >30 μ m, we simply set their equivalent pore diameters as 0.6 μ m, 15.5 μ m and 1015 μ m, respectively. The soil water characteristic curve can be measured by the pressure-membrane method, and a 10 mm in height and 50 mm in diameter soil sample should be prepared before measuring. For both of the saturated hydraulic conductivity and water characteristic curve soil samples, three replications (with a dry density of 1.35 g/cm³) are needed to minimize the measurement error.

The depth of wetting front, amount of infiltration and recording time were recorded at 30 min intervals at the beginning, at increasing intervals as the experiment progressed and at approximately 24 h intervals at the end of the experiment. We ended the experiments as the wetting front moves to the top layer for the capillary rise process and to the bottom layer (above the gravel sand layer) for the infiltration process. A balance with an accuracy of ± 0.01 g was used to measure the cumulative capillary adsorption amount during the capillary rise process. In order to understand the characteristics of capillary water rise in different periods, the capillary water rise height was arbitrarily divided into initial, steady, transition and sandy periods of capillary water rise, which indicated the 0–10 cm, 10–20 cm, 20–30 cm and 30–50 cm stages, respectively, from bottom to top. After the experiment ended, the soil moisture and electrical conductivity of the saturated extract (ECe) were measured by oven-drying method and conductivity method from 3 repeated soil samples with depths of 0–5, 5–10, 10–15, 15–20, 20–25, 25–30, 30–35, 35–40, 40–45 and 45–50 cm. The soil samples prepared for soil moisture and electrical conductivity were collected using a soil corer.

The coefficients of determination R^2 were used to evaluate the regression goodness, and the calculation of R^2 can be referred to Formulas (6)–(8):

$$R^2 = 1 - \frac{SS_{res}}{SS_{tot}} \quad (6)$$

$$SS_{tot} = \sum_{i=1}^n (y_i - \bar{y})^2 \quad (7)$$

$$SS_{res} = \sum_{i=1}^n (f_i - \bar{y})^2 \quad (8)$$

where SS_{res} means residual sum of squares, SS_{tot} means total sum of squares, \bar{y} means average value of y_i and f_i means error for y_i . The coefficient of determination R^2 is between 0 to 1, and the higher the value, the better the performance.

The statistical analyses were carried out by using SPSS (Ver. 16.0, SPSS Inc., Chicago, IL, USA). An analysis of variance (ANOVA) with least significant difference (LSD) ($p < 0.05$) was used to determine the differences between means. The distributions of soil water content, and ECe were analyzed by using Excel 2007.

3. Results and Discussion

3.1. Variation of Saturated Soil Hydraulic Conductivity and Porosity Ratio

As shown in Table 2, the saturated soil hydraulic conductivity of 10 kg/m² (U10/D10) and 20 kg/m² (U20/D20) sediment addition treatments increased significantly ($p < 0.05$), and were 3.28 and 12.06 times higher than that of 0 kg/m² (U0/D0). For 10 kg/m² (U10/D10) and 20 kg/m² (U20/D20) treatments, the ratio of macroporosity increased by 19.85% and 63.45%, respectively, while the ratio of microporosity decreased by 24.91% and 60.32%, respectively. Therefore, it can be seen that sediment addition mainly increased the macroporosity ratio and decreased the microporosity ratio, and the increase in the macroporosity ratio could increase the saturated soil hydraulic conductivity to some extent [11,23].

Table 2. Variation in saturated soil hydraulic conductivity and porosity ratio for different sediment addition.

Sediment Addition (kg/m ²)	Treatments	Saturated Soil Hydraulic Conductivity ($\times 10^3$ cm/min)	Ratio of Soil Porosity (%)		
			Macroporosity	Mesoporosity	Microporosity
0	U0/D0	0.36 c	9.52 c	13.75 a	8.67 a
10	U10/D10	1.18 b	11.41 b	12.18 ab	6.51 b
20	U20/D20	4.34 a	15.56 a	11.37 b	3.44 c

Note: Values followed by the same letter within a column are not significantly different at $p < 0.05$, as determined by the LSD test. U0/D0, U10/D10 and U20/D20 indicate the treatments of the sediment addition with 0 kg/m², 10 kg/m² and 20 kg/m², respectively.

3.2. Characteristics of Upward Water Transportation

3.2.1. Variation of Capillary Water Rise Height

It showed that the height of capillary water rise increased with time in the 0–50 cm layer, and there was no significant difference among U0, U10 and U20 at the same time (Figure 2). In the 0–10 cm soil layer, the capillary water rise height over time followed the power relationship with the determination coefficients higher than 0.99 for U0, U10 and U20 (Figure 2b). In the 10–20 cm and 20–30 cm soil layers, the capillary rise height of U0, U10 and U20 showed a linear relationship with time, and the capillary water rise height of U0 was higher than that of U10 and U20 at the same time. For the 30–50 cm soil layer, the capillary water rise height varied with time and showed a linear relationship. The actual capillary water rise height is higher than the simulated height (Figure 2e), which can be attributed to the comprehensive impact of the soil particle composition structure and soil water gravity on the soil layer with the added sediment [33].

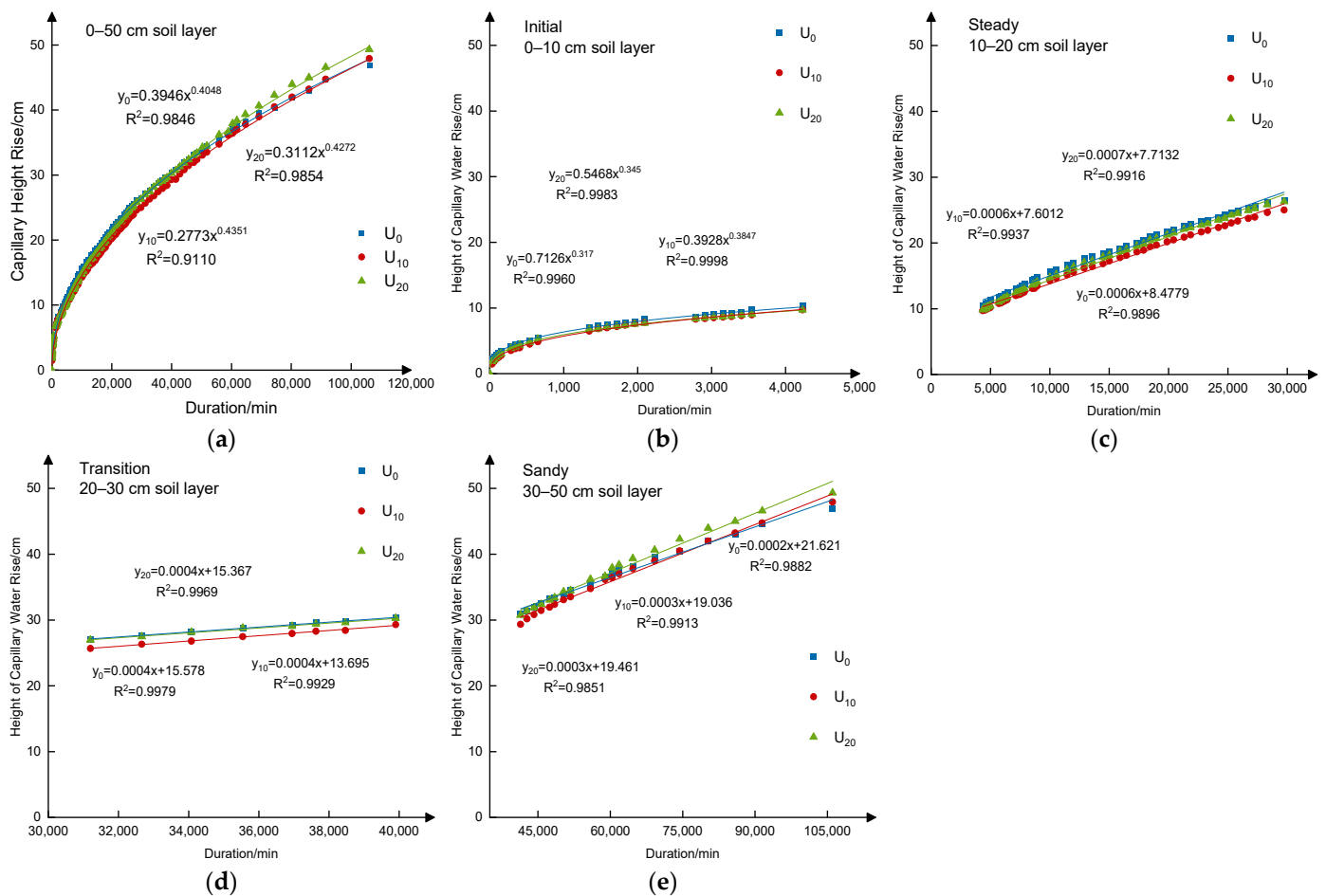


Figure 2. Variation of capillary rise height with time (a), initial (b), steady (c), transition (d) and sandy (e) period. U0, U10 and U20 indicate the upward water treatments of the sediment addition with 0 kg/m², 10 kg/m² and 20 kg/m², respectively.

3.2.2. Variation of Capillary Rise Rate

The capillary rise rate decreased rapidly in the 0–400 min period, and the capillary rise rate fluctuated within $0.1\text{--}0.5 \times 10^{-3}$ cm/min for U0, U10 and U20 (Figure 3) during the sandy period. The capillary rise rates were 74.17×10^{-3} cm/min, 49.17×10^{-3} cm/min and 61.67×10^{-3} cm/min at the beginning and were 1.8947×10^{-3} cm/min, 1.5762×10^{-3} cm/min and 1.7504×10^{-3} cm/min on average during the whole experimental period for U0, U10 and U20, respectively (Figure 3). The capillary rise rates for the beginning and the average of the three treatments were not significantly different ($p < 0.05$, Figure 3). In the 0–10 cm layer, the capillary rise rate treated by U0, U10 and U20 showed a power relationship with time, and the determination coefficients were more than 0.9. The capillary rise rate of U0 and U20 were 24.61% and 11.24% higher than those of U10 in 0–10 cm layers, and were 18.72% and 18.87% higher than those of the U10 in 10–20 cm layers, while the capillary rise rate of U10 and U20 were higher than those of U0 in both the 20–30 cm and the 30–50 cm layers (Table 3). According to the relationship between the capillary rise height and soil porosity [34], it can be seen that the sediment addition to saline–sodic soil will affect the capillary rise rate to a certain extent.

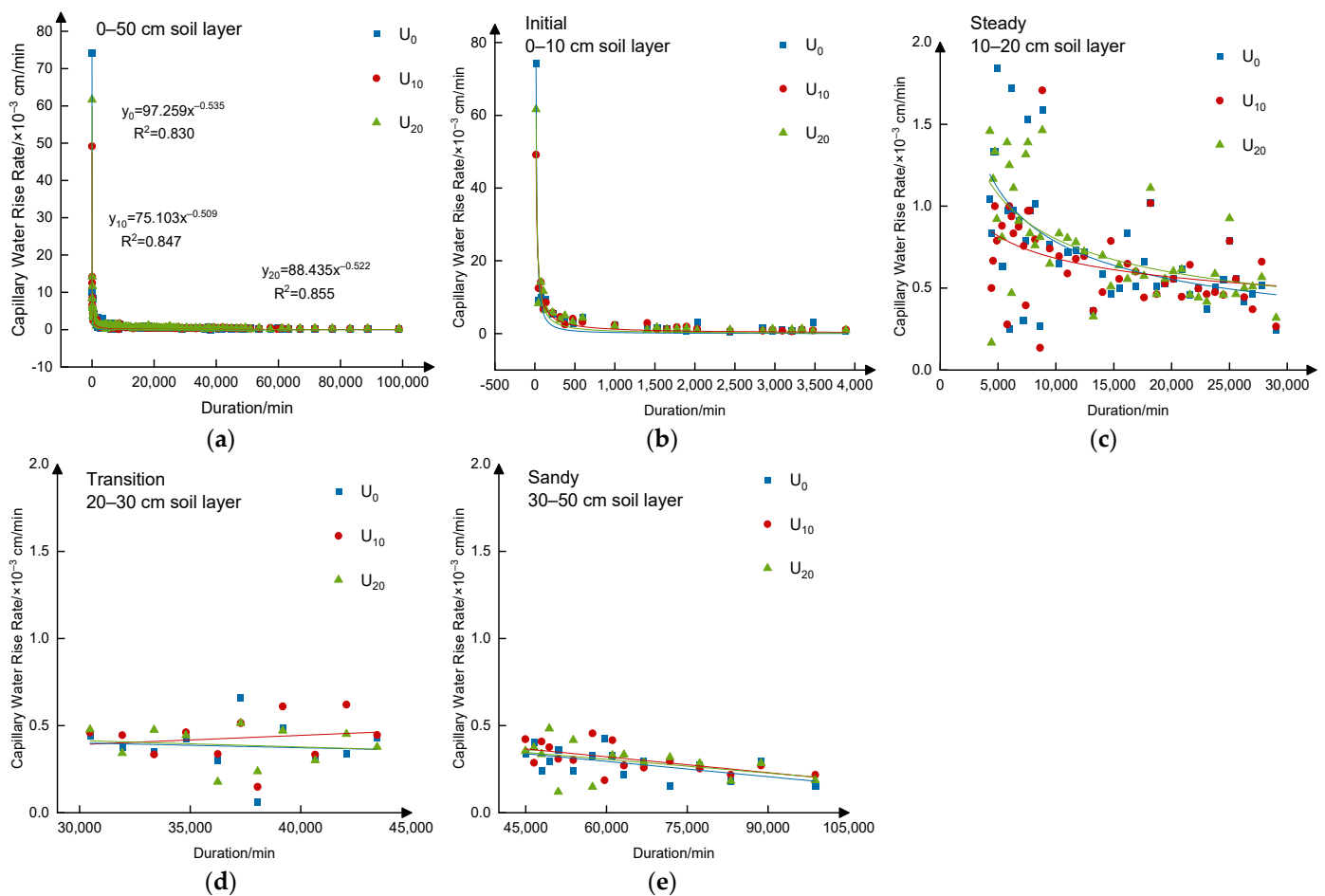


Figure 3. Variation of capillary rise rate with time (a), initial (b), steady (c), transition (d), and sandy (e) period. U0, U10 and U20 indicate the upward water treatments of the sediment addition with 0 kg/m², 10 kg/m², and 20 kg/m², respectively.

Table 3. Capillary water adsorption variation for different treatments.

Treatments	Cumulative Capillary Adsorption Amount (kg)				Capillary Rise Rate ($\times 10^{-3}$ cm/min)				Capillary Adsorption Rate ($\times 10^{-3}$ kg/min)			
	Initial 0–10 cm	Steady 10–20 cm	Transition 20–30 cm	Sandy 30–50 cm	Initial 0–10 cm	Steady 10–20 cm	Transition 20–30 cm	Sandy 30–50 cm	Initial 0–10 cm	Steady 10–20 cm	Transition 20–30 cm	Sandy 30–50 cm
U0	0.342 c	0.707 c	0.231 c	0.761 c	6.11 a	0.780 a	0.397 a	0.294 c	0.13 c	0.036 b	0.017 b	0.018 a
U10	0.373 a	0.770 a	0.27 b	0.894 b	4.90 c	0.657 b	0.412 a	0.335 a	0.19 a	0.042 ab	0.020 a	0.022 a
U20	0.355 b	0.754 b	0.285 a	0.956 a	5.49 b	0.781 a	0.412 a	0.318 b	0.17 b	0.047 a	0.019 ab	0.022 a

Note: U0, U10 and U20 indicate the upward water treatments of the sediment addition with 0 kg/m², 10 kg/m² and 20 kg/m², respectively. Values followed by the same letter within a column are not significantly different at $p < 0.05$, as determined by the LSD test.

3.2.3. Variation of Soil Water Adsorption

Similar to the variation of the capillary rise height with time, the cumulative capillary soil water adsorption with time also presents power relationship for U0, U10 and U20 (Figure 4a). Compared with U0, the cumulative capillary soil water adsorption of U10 and U20 increased by 9.06% and 3.80% for the initial period, increased by 8.91% and 6.65% for the steady period, increased by 16.88% and 23.88% for the transition period and increased by 17.48% and 25.62% for the sandy period (Table 3). The results showed that the mixed sediment layer not only increased the adsorption capacity of the mixed layer to soil water but also had a positive impact on its adjacent layers, and similar results can also be seen in Song et al.'s investigation [35].

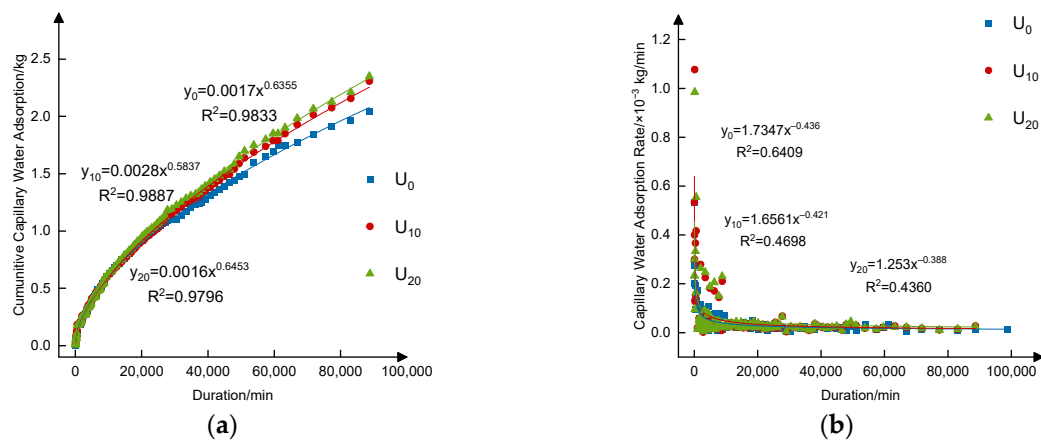


Figure 4. Variation of cumulative capillary water adsorption (a) and capillary adsorption rate (b) with time. U_0 , U_{10} and U_{20} indicate the upward water treatments of the sediment addition with 0 kg/m^2 , 10 kg/m^2 and 20 kg/m^2 , respectively.

During the capillary rise period, the soil adsorption rate showed a power formula with time for the upward water treatments (U_0 , U_{10} , U_{20}). The capillary soil water adsorption rate of each treatment decreases sharply and then tends to be stable (Figure 4b). The capillary soil water adsorption rates of U_0 , U_{10} and U_{20} were $0.200 \times 10^{-3} \text{ kg/min}$, $0.533 \times 10^{-3} \text{ kg/min}$ and $0.233 \times 10^{-3} \text{ kg/min}$ at the beginning. The capillary soil water adsorption rate varies between 0 and $0.05 \times 10^{-3} \text{ kg/min}$ with a small fluctuation amplitude during the final period. The average capillary soil water adsorption rate showed a gradual decrease for U_0 , U_{10} and U_{20} in the initial, steady, transition and sandy periods, and the average capillary soil water adsorption rate of U_{10} and U_{20} was higher than that of U_0 during the whole experimental period (Table 3), which is similar to previous studies [12,13].

3.2.4. Relationship between Capillary Rise Height and Cumulative Soil Water Adsorption Amount

The fitting results showed that there was a linear correlation ($R^2 > 0.99$) between the capillary rise height and soil water adsorption (Figure 5). The slope of the fitting equations of U_{10} and U_{20} were slightly higher than that of U_0 , which indicated that saline–sodic soil mixed with sediment could increase soil water adsorption and improve the soil water holding capacity under the same conditions of capillary rise. Similar conclusions can also be seen from Ma et al. [3] and Philip [27].

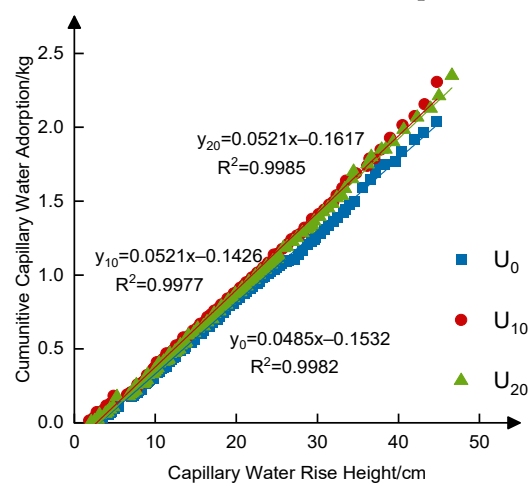


Figure 5. Relationship between the capillary rise height and the cumulative adsorption water amount. U_0 , U_{10} and U_{20} indicate the upward water treatments of the sediment addition with 0 kg/m^2 , 10 kg/m^2 and 20 kg/m^2 , respectively.

3.3. Characteristics of Downward Soil Water Transportation

3.3.1. Wetting Front Migration

In the 0–50 cm soil layer, the wetting front migration is positively correlated with time. The determination coefficients (R^2) of D0, D10 and D20 are greater than 0.97, and the slopes of D10 and D20 are greater than that of D0, which indicates that the infiltration rate of D10 and D20 is high (Figure 6a). This can be attributed to the ratio of the macroporosity increase with the addition of sediment. However, in the 0–20 cm soil layer, the infiltration wetting front showed an exponential relationship with time, and the determination coefficients were all above 0.99 for D0, D10 and D20 (Figure 6b). Furthermore, a positive correlation was shown in the 20–50 cm layer with the determination coefficients of 0.993, 0.9878 and 0.9935 for D0, D10 and D20, respectively (Figure 6c). The simulation of piecewise functions is better than full-time simulation, which is similar to Mathur et al. [21] and Gan et al. [36]. The difference of the fitting curve among the D0, D10 and D20 treatments at different soil layers can mainly be attributed to the air resistance as poor ventilation inside the soil [30].

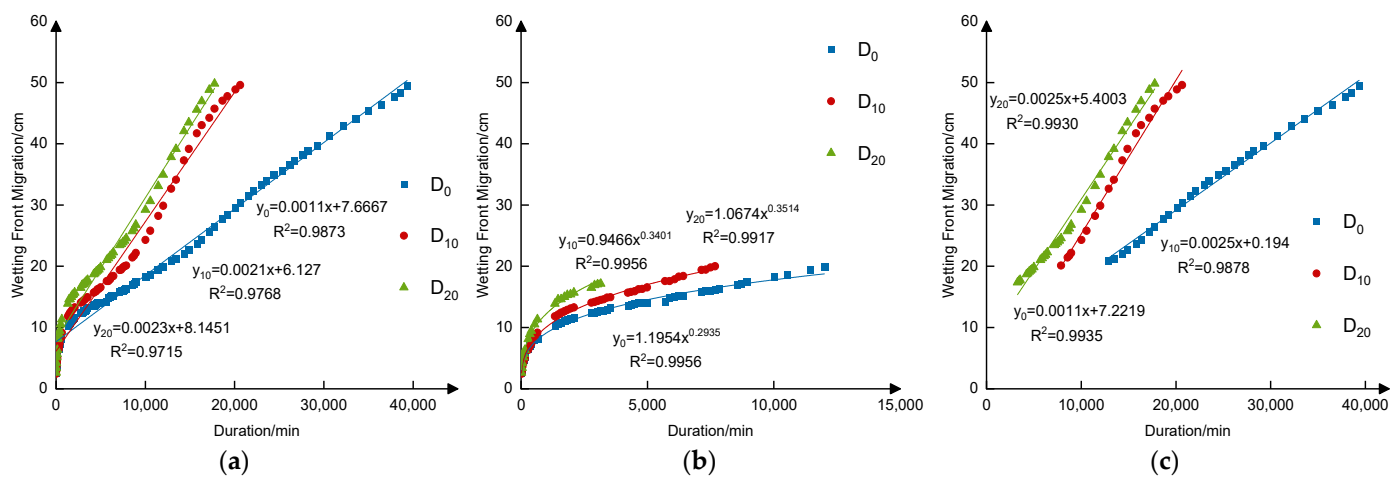


Figure 6. Variation of soil wetting front migration with time (a), 0–20 cm soil layer (b), 20–50 cm soil layer (c). D0, D10 and D20 indicate the downward water treatments of the sediment addition with 0 kg/m², 10 kg/m² and 20 kg/m², respectively.

Under the condition of constant head infiltration, it takes 12,000 min, 7675 min and 4985 min to migrate from the surface to 20 cm depth for D0, D10 and D20, respectively (Figure 6b). The time required for D0 was approximately 1.56 and 2.41 times higher than that of D10 and D20, respectively. Moreover, it takes 27,331 min, 12,960 min and 12,770 min for the wetting front to move from the 20 cm to 50 cm depth for D0, D10 and D20, respectively (Figure 6c). These results indicate that sediment addition to the saline-sodic soil not only improved the wetting front migration rate in the mixed layers but also improved the migration rate of the wetting front in unmixed soil layer, which is similar to Song et al. [35] and Mathur et al. [21].

3.3.2. Soil Water Infiltration Rate

In the 0–20 cm layer, the infiltration rates of D0, D10 and D20 were rapidly reduced from 176.67×10^{-3} cm/min, 163.3×10^{-3} cm/min and 175.0×10^{-3} cm/min at the beginning to 0.963×10^{-3} cm/min, 1.111×10^{-3} cm/min and 1.974×10^{-3} cm/min at the end, which were reduced by 183.46, 147.01 and 88.65 times, respectively (Figure 7a). The average infiltration rates of the 0–20 cm layer for D0, D10 and D20 were 7.834×10^{-3} cm/min, 8.733×10^{-3} cm/min and 13.254×10^{-3} cm/min, respectively. The infiltration rate of the three treatments initially increased and then decreased with time in the 20–50 cm layer (Figure 7b), and D10 and D20 both reached a maximum infiltration rate at 13,887 min (corresponding to infiltration depths of 37.5 cm and 42.5 cm, respectively), while D0 reached a maximum infiltration rate at 20,000 min (corresponding to an infiltration depth of 25.6 cm).

During the water infiltration progress, the average infiltration rate of D0 was significantly lower than those of D10 and D20 in the 20–50 cm layer (which were 1.10×10^{-3} cm/min, 2.16×10^{-3} cm/min and 2.19×10^{-3} cm/min for D0, D10 and D20, respectively). In the 0–50 cm layer, the average infiltration rates for D0, D10 and D20 were 4.936×10^{-3} cm/min, 6.560×10^{-3} cm/min and 8.315×10^{-3} cm/min, respectively.

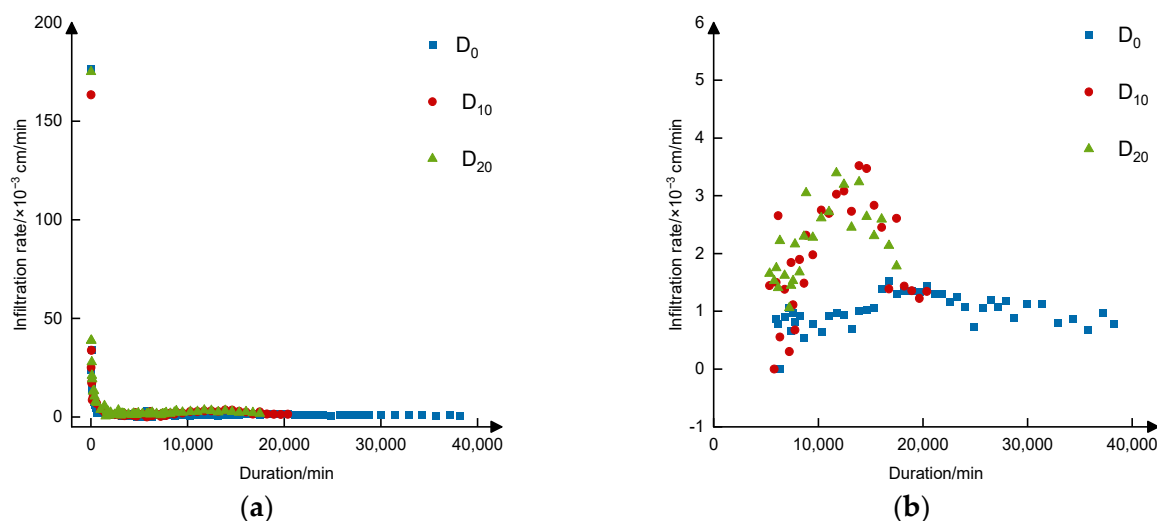


Figure 7. Variation of soil infiltration rate with time (a) and detail variation of relative low infiltration rate from 5700 min to the final period (b). D0, D10 and D20 indicate the downward water treatments of the sediment addition with 0 kg/m², 10 kg/m² and 20 kg/m², respectively.

Considering the effect of capillary water gravity, the soil infiltration rates of D0, D10 and D20 showed significant differences ($p < 0.05$). The infiltration rate of D0, D10 and D20 increased first and then decreased, and the infiltration rates of D10 and D20 were significantly higher than D0 (Figure 7b). This can be explained by the theory of soil liquid and air exchange during the infiltration process: soil air gradually migrates to the bottom and is replaced by water [37]. Moreover, this phenomenon may also be related to the water conductivity and air conduction performance of the bottom filter layer (thickness, filter gradation) [38,39].

3.4. Comparison of Downward and Upward Soil Water Movement

3.4.1. Duration Time

For the process of water capillary rise and infiltration, the initial capillary water absorption/infiltration rate of soil is much higher than that in the steady state, which is due to the low soil water content and high soil water absorption in the initial state [40,41]. The water conveyance time to pass through the 50 cm height soil column for U0, U10 and U20 is 2.5, 4.9 and 5.7 times higher than that of D0, D10 and D20, respectively, which can be attributed to the water gravity resistance in the process of capillary water rise. Moreover, we can also see that the effect of sediment addition on water infiltration is more obvious than that of capillary rise, and the greater the sediment addition, the shorter the infiltration time. This is because with the sediment addition, both the soil-saturated hydraulic conductivity and macroporosity are increased (Table 2).

3.4.2. Soil Water and Salt Distribution

The distribution of soil water and salt after the capillary rise/infiltration process are shown in Figure 8. It can be seen that the soil moisture of D0, D10 and D20 decreases from the surface to the bottom layer (Figure 8a), while the soil E_c increases with the increase in soil depth (Figure 8b). The distribution results of soil moisture and E_c in U0, U10 and U20 were opposite with those of D0, D10 and D20 (Figure 8). The soil water moisture

distribution of capillary rise and infiltration was symmetrically distributed at $x = 32\%$ m/m, and the soil ECe was symmetrically distributed with $y = 25$ cm. However, the distributions of both the soil moisture and ECe for water capillary rise and infiltration process are not strictly symmetrical. In the 0–50 cm soil layer, the average soil moisture of downward treatments (D0, D10, D20) is 17.81% higher, and the average ECe is 31.47% lower than that of the upward treatments (U0, U10, U20), mainly because the duration time for the upward water treatments (U0, U10, U20) is relatively long and the cumulative evaporation amount is relatively high compared with the downward treatments (D0, D10, D20).

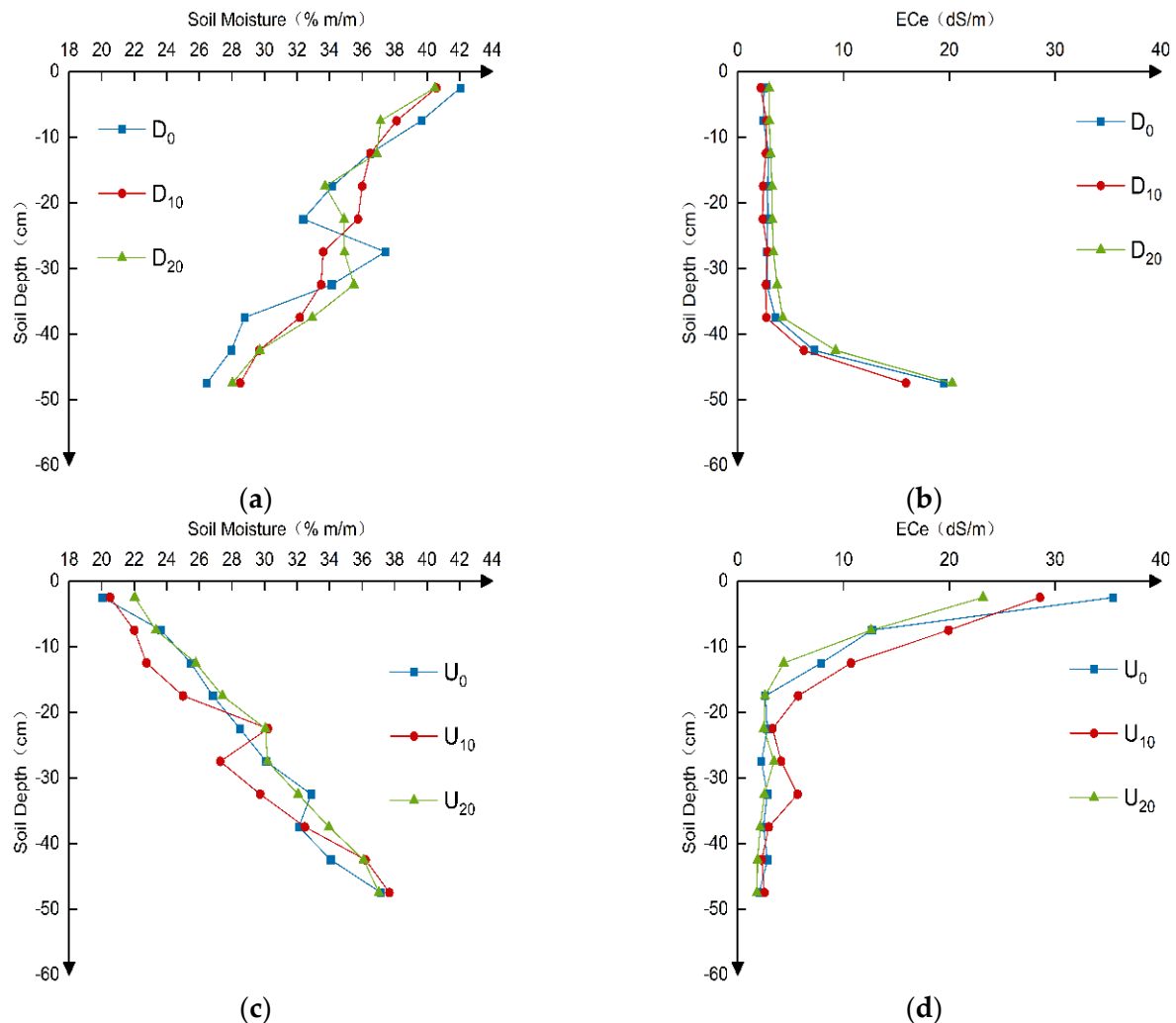


Figure 8. Distribution of soil moisture (a,c) and saturated extract electrical conductivity (ECe) (b,d) for downward/upward water treatments. D0, D10 and D20 indicate the sediment addition treatments with 0 kg/m^2 , 10 kg/m^2 and 20 kg/m^2 , respectively, for downward water; U0, U10 and U20 indicate the sediment addition treatments with 0 kg/m^2 , 10 kg/m^2 and 20 kg/m^2 , respectively, for upward water.

3.5. Modeling of Soil Water Infiltration and Capillary Water Rise

The wetting front migration rate for soil water infiltration and capillary water rise were simulated with the Kostiakov, Philip, and Horton models, and the results are shown in Table 4. We can see that the Philip model performs the best among the three models in fitting both the upward and downward water process of saline-sodic soil, with the R^2 all above 0.74, while the average R^2 of the Horton model was the lowest among the three models, indicating that the Philip model can simulate both upward and downward water migration processes. Moreover, we can also see that the Kostiakov model performs better

in the upward treatments (U0, U10 and U20) than the downward treatments (D0, D10 and D20), which is mainly because of the air resistance and the complicated pore distribution structure [37,39].

Table 4. Simulation results of soil water infiltration and capillary water rise model.

Treatments	Kostiakov	R^2	Philip	R^2	Horton	R^2
U0	$y = 97.259 \times x^{-0.535}$	0.8302	$y = 194.77 \times x^{-0.5} - 1.6794$	0.7477	$y = 17.23 \times \text{EXP}(-0.001 \times x) + 0.2491$	0.3184
U10	$y = 75.103 \times x^{-0.509}$	0.8478	$y = 146.95 \times x^{-0.5} - 1.0253$	0.8713	$y = 16.106 \times \text{EXP}(-0.001 \times x) + 0.2586$	0.3837
U20	$y = 88.435 \times x^{-0.522}$	0.8551	$y = 171.57 \times x^{-0.5} - 1.3432$	0.8013	$y = 14.444 \times \text{EXP}(-0.001 \times x) + 0.2755$	0.4576
D0	$y = 87.723 \times x^{-0.479}$	0.706	$y = 360.38 \times x^{-0.5} - 4.7121$	0.8017	$y = 116.96 \times \text{EXP}(-0.0015 \times x) + 0.6528$	0.6868
D10	$y = 164.21 \times x^{-0.598}$	0.609	$y = 344.85 \times x^{-0.5} - 4.7347$	0.8242	$y = 109.77 \times \text{EXP}(-0.0015 \times x) + 1.3804$	0.701
D20	$y = 176.56 \times x^{-0.519}$	0.6738	$y = 392.07 \times x^{-0.5} - 5.2418$	0.8849	$y = 125.33 \times \text{EXP}(-0.0015 \times x) + 1.9791$	0.7658

Note: U0, U10 and U20 indicate the treatments of the sediment addition with 0 kg/m², 10 kg/m² and 20 kg/m², respectively, for upward water; D0, D10 and D20 indicate the downward water treatments of the sediment addition with 0 kg/m², 10 kg/m² and 20 kg/m², respectively, for downward water.

4. Conclusions

The results showed that with the increase in sediment addition, both the macroporosity ratio and saturated soil hydraulic conductivity of the mixed soil increased. The addition of sediment significantly increased the soil water wetting front migration rate and promoted the soil water adsorption amount. A liner relationship was established between the capillary rise height and soil cumulative water absorption amount. The Philip model is more suitable for both modelling the capillary water rise and soil water infiltration process. Considering the water and salt distribution after the infiltration/capillary rise process, the 20 kg/m² sediment addition seems to be more helpful to promote salt leaching or prevent salt accumulation. As the dynamics of soil water and salt movement are influenced by various factors, further study needs to be conducted.

Author Contributions: Conceptualization, C.S. and M.Z.; methodology, C.S. and P.Z.; validation, D.F. and C.Y.; formal analysis, X.H. and X.S.; investigation, J.S.; resources, H.H. and J.S.; data curation, W.M.; writing—original draft preparation, C.S. and M.Z.; writing—review and editing, C.S. and P.Z.; visualization, C.Y.; supervision, J.S.; project administration, C.S., M.Z. and P.Z.; funding acquisition, C.S. and M.Z. All authors have read and agreed to the published version of the manuscript.

Funding: This study was supported by the National Natural Science Foundation of China (No. 52109059, 32001473), the Natural Science Foundation of Shandong Province (No. ZR2018BEE048, ZR2019PC008), the Shandong Provincial Key Research and Development Program-Major Scientific and Technological Innovation Project (No. 2019JZZY010727) and the Zhongke Shandong Dongying Institute of Geographic Sciences Open Fund (No. 202104).

Data Availability Statement: The data presented in this study are available on request from the corresponding author.

Acknowledgments: The authors are grateful to editors and reviewers for their constructive comments and suggestions on this manuscript.

Conflicts of Interest: The authors declare no conflict of interest.

References

1. Cui, B.; Yang, Q.; Yang, Z.; Zhang, K. Evaluating the ecological performance of wetland restoration in the Yellow River delta, China. *Ecol. Eng.* **2009**, *35*, 1090–1103. [\[CrossRef\]](#)
2. Peng, J.; Chen, S.; Dong, P. Temporal variation of sediment load in the yellow river basin, china, and its impacts on the lower reaches and the river delta. *Catena* **2010**, *83*, 135–147. [\[CrossRef\]](#)
3. Ma, T.; Li, X.; Bai, J.; Ding, S.; Zhou, F.; Cui, B. Four decades' dynamics of coastal blue carbon storage driven by land use/land cover transformation under natural and anthropogenic processes in the yellow river delta, China. *Sci. Total Environ.* **2019**, *655*, 741–750. [\[CrossRef\]](#) [\[PubMed\]](#)
4. Guan, Y.; Liu, G. Remote sensing detection of dynamic variation of the saline land in the yellow river delta. *Remote Sens. Nat. Resour.* **2003**, *15*, 19–22+33.

5. Xiao, Y.; Zhao, G.; Li, T.; Zhou, X.; Li, J. Soil salinization of cultivated land in Shandong province, China—Dynamics during the past 40 years. *Land Degrad. Dev.* **2019**, *30*, 426–436. [[CrossRef](#)]
6. Li, X.; Wan, S.; Kang, Y.; Chen, X.; Chu, L. Chinese rose (*Rosa chinensis*) growth and ion accumulation under irrigation with waters of different salt contents. *Agric. Water Manag.* **2016**, *163*, 180–189. [[CrossRef](#)]
7. Yu, S.; Liu, J.; Eneji, A.; Han, L.; Tan, L.; Liu, H. Dynamics of soil water and salinity under subsurface drainage of a coastal area with high groundwater table in spring and rainy season. *Irrig. Drain.* **2016**, *65*, 360–370. [[CrossRef](#)]
8. Zhao, Y.; Wang, S.; Li, Y.; Zhuo, Y.; Liu, J. Effects of straw layer and flue gas desulfurization gypsum treatments on soil salinity and sodicity in relation to sunflower yield. *Geoderma* **2019**, *352*, 13–21. [[CrossRef](#)]
9. Berezniak, A.; Ben-Gal, A.; Mishael, Y.; Nachshon, U. Manipulation of soil texture to remove salts from a drip-irrigated root zone. *Vadose Zone J.* **2018**, *17*, 170019. [[CrossRef](#)]
10. Li, X.Y. Gravel–sand mulch for soil and water conservation in the semiarid loess region of northwest china. *Catena* **2002**, *52*, 105–127. [[CrossRef](#)]
11. Sun, J.; Kang, Y.; Wan, S. Effects of an imbedded gravel–sand layer on reclamation of coastal saline soils under drip irrigation and on plant growth. *Agric. Water Manag.* **2013**, *123*, 12–19. [[CrossRef](#)]
12. Zhang, Y.; Li, H.; Hong, H.; Wang, X.; Chen, W. Punching and filling sand method increasing water infiltration and desalting rate of saline-alkali soil under flooding irrigation. *Trans. CSAE* **2017**, *433*, 76–83. [[CrossRef](#)]
13. Nie, J.; Stevens, T.; Rittner, M.; Stockli, D.; Pan, B. Loess plateau storage of northeastern Tibetan plateau-derived Yellow River sediment. *Nat. Commun.* **2015**, *6*, 8511. [[CrossRef](#)]
14. Dai, Q.; Cao, W.H.; Shi, H.L.; Wang, Y.H. Analyses on some problems in irrigation districts and benefits of allocating diverted water and sediment along the lower yellow river. *J. China Inst. Water Resour. Hydropower Res.* **2007**, *5*, 15–20. [[CrossRef](#)]
15. Wang, Q.; Shao, M.A.; Wang, Z. Mechanism and simulating model for muddy water infiltration. *Trans. CSAE* **1999**, *15*, 135–138.
16. Yao, X.; Li, J.; Huang, X.; Sun, X. Distribution of yellow river’s silt in field under border irrigation. *Trans. CSAE* **2016**, *32*, 147–152. [[CrossRef](#)]
17. Liu, L.; Niu, W.; Wu, Z.; Olusola, O.; Guan, Y. Effect of fertilization and sediment flow hydraulic characteristics on emitter clogging in muddy water drip fertigation system. *Irrig. Drain.* **2018**, *67*, 713–723. [[CrossRef](#)]
18. Mao, W.; Kang, S.; Wan, Y.; Sun, Y.; Wang, Y. Yellow river sediment as a soil amendment for amelioration of saline land in the yellow river delta. *Land Degrad. Dev.* **2016**, *27*, 1595–1602. [[CrossRef](#)]
19. Alqahtani, M.R.A. Effect of addition of sand and soil amendments to loam and brick grit media on the growth of two turf grass species (*Lolium perenne* and *Festuca rubra*). *J. Appl. Sci.* **2009**, *9*, 2485–2489. [[CrossRef](#)]
20. Li, W.; Li, X.; Li, H.; Yang, Y.; Lei, K.; Yao, X. Effects on micro-ecological characteristics in clayey soil of tobacco area under different sand adding proportions. *J. Northwest Agric. For. Univ. Sci. Technol. Nat. Sci. Ed.* **2012**, *40*, 85–96. [[CrossRef](#)]
21. Mathur, O.P.; Mathur, S.K.; Talati, N.R. Effect of addition of sand and gypsum to fine-textured salt-affected soils on the yield of cotton and jower (*Sorghum*) under Rajasthan Canal Command Area conditions. *Plant Soil* **1983**, *74*, 61–65. [[CrossRef](#)]
22. Zhou, L.; Li, R.; Miao, Q.; Dou, X.; Tian, F.; Yu, D.; Sun, C. Effects of different sand ratios on infiltration and water-salt movement of heavy saline-alkali soil in Hetao irrigation area. *Trans. CSAE* **2020**, *36*, 116–123. [[CrossRef](#)]
23. Kostiaikov, A. On the dynamics of the coefficient of water percolation in soils and on the necessity of studying it from a dynamic point of view for purposes of amelioration. *Trans. 6th Comm. Int. Soc. Soil Sci. Russ.* **1932**, *1*, 17–21.
24. Horton, R.E. The role of infiltration in the hydrologic cycle. *Trans. Am. Geophys. Union* **1933**, *14*, 446–460. [[CrossRef](#)]
25. Horton, R.E. Analysis of runoff-plat experiments with varying infiltration-capacity. *Trans. Am. Geophys. Union* **1939**, *20*, 693–711. [[CrossRef](#)]
26. Philip, J. The theory of infiltration: 4. Sorptivity and algebraic infiltration equations. *Soil Sci.* **1957**, *84*, 257–264. [[CrossRef](#)]
27. Philip, J. The theory of infiltration: 7. *Soil Sci.* **1958**, *85*, 333–337. [[CrossRef](#)]
28. Al-Dosary, N.; Al-Sulaiman, M.A.; Aboukarima, A.M. Modelling the unsaturated hydraulic conductivity of a sandy loam soil using Gaussian process regression. *Water SA* **2019**, *45*, 121. [[CrossRef](#)]
29. Zolfaghari, A.A.; Mirz, E.S.; Gorji, M. Comparison of Different Models for Estimating Cumulative Infiltration. *Int. J. Soil Sci.* **2012**, *7*, 108–115. [[CrossRef](#)]
30. Wang, P.; Jiang, E.; Zhang, Q. Study on the Benefits of Sediment Recycling Model in Yellow River Irrigation District. *Yellow River* **2010**, *32*, 143–144. [[CrossRef](#)]
31. Nimmo, J.R. Porosity and Pore Size Distribution. In *Encyclopedia of Soils in the Environment*; Hillel, D., Ed.; Elsevier: Amsterdam, The Netherlands, 2004; Volume 3, pp. 295–303. [[CrossRef](#)]
32. Rabot, E.; Wiesmeier, M.; Schlüter, S.; Vogel, H.J. Soil structure as an indicator of soil functions: A review. *Geoderma* **2018**, *314*, 122–137. [[CrossRef](#)]
33. He, F.; Pan, Y.; Tan, L.; Zhang, Z.; Li, P.; Liu, J. Study of the water transportation characteristics of marsh saline soil in the yellow river delta. *Sci. Total Environ.* **2017**, *574*, 716–723. [[CrossRef](#)] [[PubMed](#)]
34. Li, P.; Pan, Y.H.; He, F.H.; Tan, L.L.; Ji, S.X. Research on capillary water adsorption characteristics of yellow river delta wetland soil. *Chin. J. Agrometeorol.* **2017**, *38*, 378–387. [[CrossRef](#)]
35. Song, R.; Chu, G.; Ye, J.; Bai, L.; Zhang, R.; Yang, J. Effects of surface soil mixed with sand on water infiltration and evaporation in laboratory. *Trans. CSAE* **2010**, *26*, 109–114.

36. Gan, Y.; Liu, H.; Jia, Y.; Zhao, S.; Wei, J.; Xie, H. Infiltration-runoff model for layered soils considering air resistance and unsteady rainfall. *Hydrol. Res.* **2019**, *50*, 431–458. [[CrossRef](#)]
37. White, I.; Sully, M. Macroscopic and microscopic capillary length and time scales from field infiltration. *Water Resour. Res.* **1987**, *23*, 1514–1522. [[CrossRef](#)]
38. Li, Y.N. Study on the effect of muddy irrigation on soil air pressure. *Agric. Res. Arid. Areas* **2003**, *21*, 91–93.
39. Rodgers, M.; Mulqueen, J.; Healy, M. Surface clogging in an intermittent stratified sand filter. *Soil Sci. Soc. Am. J.* **2004**, *68*, 1827. [[CrossRef](#)]
40. Hu, H.; Mao, X.; Barry, D.; Liu, C.; Li, P. Modeling reactive transport of reclaimed water through large soil columns with different low-permeability layers. *Hydrogeol. J.* **2015**, *23*, 351–364. [[CrossRef](#)]
41. Liu, B.; Wang, S.; Kong, X.; Liu, X. Soil matric potential and salt transport in response to different irrigated lands and soil heterogeneity in the North China Plain. *J. Soils Sediments* **2019**, *19*, 3982–3993. [[CrossRef](#)]